Astronomy & Astrophysics manuscript no. sn2011dh-1-v1
May 6, 2012

Optical and near-infrared observations of SN 2011dh - Day 1 - 100.

M. Ergon[1]

[1] Oskar Klein Centre, Department of Astronomy, AlbaNova, Stockholm University, 106 91 Stockholm, Sweden
[2] Astrophysics Research Center, School of Mathematics and Physics, Queen's University Belfast, Belfast, BT7 1NN, Northern Ireland

Submitted to Astronomy and Astrophysics

ABSTRACT

We present optical and near-infrared (NIR) photometry and spectroscopy of the Type IIb supernova (SN) 2011dh for the first 100 days. Except for presentation and discussion of the data the main objective of this paper is to build the bolometric lightcurve using our dataset complemented with SWIFT ultra-violet (UV) and Spitzer mid-infrared (MIR) data. Hydrodynamical modeling of the SN based on this bolometric lightcurve is presented in Bersten et al (2012). This is the first in a series of papers presenting the photometric and spectroscopic evolution in optical and NIR as well as detailed analysis and modeling of the SN.

Key words. supernovae: general — supernovae: individual (SN 2011dh) — galaxies: individual (M51)

1. Introduction

Core-collape (CC) SNe are caused by the gravitational collapse of the iron core in massive stars. The diversity of the events that we observe reflects the diversity of the progenitor stars and the surrounding circum-stellar media. In particular the extent to which the star has lost its hydrogen envelope has a profund impact of the observed properties of the SN. Stars that have retained their hydrogen envelope tend to produce SNe that remain bright for a longer time, have lower expansion velocities and from the usually strong hydrogen lines present in their spectra they are classified as Type II SNe. Stars that have lost their hydrogen envelope tends to produce SNe that fade faster, have higher expansion velocities and from the abscence of hydrogen lines in their spectra they are classified as Type I SNe. The designation IIb are used for SNe which shows a spectral transition from Type II at early times to Type Ib at later times. These SNe are thought to arise from stars that lost most but not all of their hydrogen envelope.

Despite the greatly improved understanding of the physics driving CC SNe during the last decades the connection between the observed properties of SNe and their progenitor stars are still not well understood. Identification of the progenitor stars themselfs in archive images has become increasingly feasible in the last decade because of growing data archives and improved observing techniques. By comparison of the magnitude and colour of the star to predictions from stellar evolutionary models basic properties as the initial mass can be estimated. High quality multi wavelength monitoring of these naturally nearby and bright SNe followed by detailed modeling of the data are crucial to our understanding of the SNe-progenitor connection. This paper will present the first 100 days of the extensive optical and NIR dataset we have obtained for SN 2011dh. The remaining data will be presented in the second paper in the series and the detailed modeling in the last.

SN 2011dh was discovered by A. Riou June 31.893 2011 (Rieland et al. 2011) in the nearby galaxy M51 at a distance of about 8 Mpc. The latest non-detecion reported in the litterature is by PFT (Palomar Transient Factory) from May 31.275 (Arcavi et al. 2011). However, there is amateur images which constrain this already small time-window even further. In this paper we will adopt May 31.5 as the epoch of explosion.

The host galaxy M51, also known as the whirpool galaxy, was the first one for which the spiral structure was observed by Lord Rosse in 1845 and is one of the most frequencly observed, both by amateurs and professionals. Thus it's not surprising that excellent pre-explosion data were available in the HST archive. Maund et al. (2011) used this to identify a yellow supergiant progenitor candidate which, by comparision to stellar evolutionary models, corresponds to a star of $13 \pm 3 M_{\odot}$ initial mass. A similar analysis by Van Dyk et al. (2011) estimated an initial mass between $17 M_{\odot}$ and $19 M_{\odot}$, the difference mainly steaming from the different method used to identify the evolutionary track in the HR-diagram.

Since the discovery the SN has been extensively monitored from X-ray to radio wavelengths by several teams. Optical and NIR photometry and spectroscopy has been published in Arcavi et al. (2011) and Maund et al. (2011). Radio observations have been published in Soderberg et al. (2011, Krauss et al. (2012) and Bietenholtz et al. (2012) and X-ray observations in Soderberg et al. (2011). The SN have been monitored in X-rays as well as UV by SWIFT, in mid-infrared (MIR) by Spitzer and at sub-millimeter wavelengths by Herschel.

The objective of this paper is to present and describe data for the first 100 days and to build the bolometric lightcurve used for hydrodynamical modeling in Bersten et al. (2012). In Sect. we will describe how the data was reduced and ...

2. Host galaxy properties

2.1. Distance

In table 1 we list all estimates for the distance of M51 we have found in the litterature. In this paper we will use assume a distance of $7.8^{+1.1}_{-0.9}$ Mpc as calculated from the 50 (median), 16 and 84 percentiles of these values (as would be approperiate for a gaussian distribution). The use of percentiles is motivated by the unsensitivity to outliers as compared to a mean and a root mean square.

Table 1. Distance to M51. Litterature values.

D(Mpc)	Method	Reference
9.60 ±0.80	Size of HII regions	Sandage & Tammann (**?**)
6.91 ±0.67	Young stellar clusters	Georgiev et al. (1990)
8.39 ±0.60	Planetary nebulae luminosity function	Feldmeier et al. (1997)
7.62 ±0.60	Planetary nebulae luminosity function	Ciardullo et al. (2002)
7.66 ±1.01	Surface brightness fluctuatons	Tonry et al. (2001)
7.59 ±1.02	Expanding photosphere method (2005cs)	Takats et al. (2006)
6.36 ±1.30	Type IIP SNe standard candle method (2005cs)	Takats et al. (2006)
8.90 ±0.50	Spectral expanding photosphere method (2005cs)	Dessart et al. (2008)
6.92 ±0.00	Type Ic SNe ... (1994I)	Iwamoto & Nomoto (1994)
7.90 ±0.70	Spectral expanding photosphere method (SN 2005cs)	Baron et al. (2007)
6.02 ±1.92	Spectral expanding photosphere method (SN 1994I)	Baron et al. (1996)
8.36 ±0.00	Type IIP SNe standard candle method (2005cs)	Poznanski et al. (2009)
9.30 ±0.00	Tully-Fisher relation	Tully (**?**)
8.40 ±0.7	Expanding photosphere method (2005cs and 2011dh)	Vinko et al. (2012)

2.2. Extinction

The interstellar exinction along the line of sight in the Milky Way as given by the extinction maps presented by Schlegel et al. (1998) is $E(B\text{-}V)$=0.035. These extinction maps were derived from 100 micron dust emission maps in turn constructed from IRAS and COBE data. Arcavi et al. (2011) obtained high-resolution spectroscopy of the SN, measured the equivalent width of the NaI D 5890 and 5896 Å lines to 188 and 107 mÅ respectively and determined the host galaxy extinction using the correlation presented by Munari & Zwitter (1997) to $E(B\text{-}V)$<0.05 mag. Similar equivalent widths of the NaI D lines were measured from high-resolution spectra by Ritchey et al. (2012) who also argue that the SN lies in front of the bulk the disk. Imaging of the SN site in the 100 micron range by Herschel also suggests a low extinction. !Approximate calculation here?! !And what about the Spitzer imaging that Van Dyk refered to?! !Estimate from the colours of local supergiants here! On the other hand, as will be discussed in Sect. 3.4, comparison of the SN to the similar Type IIb SNe 1993J and 2008ax suggests a significant extinction. However, without detailed spectral modeling it's not possible to exclude an intrinsic colour difference so we will assume a neglible host galaxy extinction and use the galactic value (see above) throughout this paper. To calculate the extinction as a function of wavelength we have used the reddening law of Cardelli et al. (1989). For broad-band photometry extinction were calulated at the effective wavelength of the filters.

3. Observations

3.1. Photometric observations

A extensive campaign of optical and NIR photometric observations was initiated for SN 2011dh shortly after discovery using a multitude of different instruments. Data have been obtained by the Liverpool Telescope (LT), the Nordic Optical Telescope (NOT), Telescopio Nazionale (TNG), Telescopio Carlos Sanchez (TCS), the Calar Alto 3.5 and 2.2m telescopes, the Asiago Schmidt telescope, the William Herschel telescope (WHT) and the Large Binocular Telescope (LBT).

3.1.1. Reductions

The optical data were reduced with the IRAF based QUBA pipeline (Stefano Valenti et al. 2011) except for the LT data for which the automatic telescope pipeline reductions have been used.

NIR data was reduced with a IRAF based pipeline written in python except for UKIRT data for which the reductions provied by CASU have been used. Except for the standard procedures (e.g. flatfielding and sky subtraction) the pipeline have support for second pass sky subtraction using an object mask, correction for field distortion and unsharp masking. Correction for field distortion is neccesary to allow co-addition of images with large dithering shifts and has been applied for the TNG data. Unsharp masking removes large scales structures (e.g. the host galaxy) in the images to facilitate the constuction of a master sky in the case of large scale structure overlap. Given the (usually) small fields of view and the large size of the host galaxy this technique have been applied to all data were seperate sky frames were not obtained. TNG data were preprocessed to remove quadrant crosstalk and WHT data were preprocessed to descramble pixel locations.

3.1.2. Photometry

Photometry have been performed with an IRAF based pipeline written in python. Given the large amount of data photometry of individual epochs is not feasible. Instead the pipeline performs photometry given a number of configuration paramaters for each telescope and instrument used. We have used aperture photometry on the reference stars as well as the SN using a relatively small aperture (1.5-2.0 times the FWHM). A mild (>0.1 mag error) rejection of the reference stars as well as a mild (3 σ) rejection of the calculated zero points were also performed.

The optical photometry were calibrated to the Johnsson-Cousine (UBVRI) system using the reference stars presented in Pastorello et al. (2009) and to the sloan (gz) system using the same reference stars. The UBVRI magnitudes for the reference stars were adopted Pastorello et al. (2009) and their gz magnitudes were calibrated using standard fields obtained on a number of photometric nights with the LT. The NIR photometry were calibrated to the 2 Micron All Sky Survey (2MASS) system using 10 stars from the 2MASS catalogue (Skrutskie et al. 2006), including the same reference stars as used for the optical calibration. Average colour constants to tansform from instrumental to standard system magnitudes have been calculated for each telescope and intrument from standard fields and are listed in Table 2, 3 and 4. The reference stars are shown in Fig. 1 and their coordinates and magnitudes listed in Table 5, 6 and 7.

We have also performed photometry on the Spitzer 3.6 and 4.5 micron imaging obtained through the DDT program by G. Helou and the SWIFT UV imaging. For the Spitzer imaging we have performed aperture photometry using the pipeline described above and used the zero points and aperture corrections provided in the IRAC Instrument Handbook to calculate intrumental IRAC magnitudes. For the SWIFT imaging we have used the UVOTIMSUM and UVOTSOURCE tools included in the HEASOFT package to determine instrumental UVOT magnitudes.

3.1.3. Results

The apparent optical and NIR magnitudes and their corresponding errors are listed in Table 8, Table 9 and Table 10 and shown in Fig .2. They are also available for download in machine readable format in the online version of the paper as well as from the WISEASS database. The Spitzer 3.6 and 4.5 micron magnitudes and their corresponding errors are listed in Table 11 and shown together with the NIR photometry in Fig. 3. It's interesting to note the markedly slower decline in the 4.5 micron band as compared to the 3.6 micron and the NIR bands. Varm dust or CO fundamental band emission are two possible explanations and we will discuss this issue further in Sect. 4. The SWIFT UV magnitudes and corresponding errors are listed in Table 12 and shown in Fig. 4. Unfortunately the response functions of the SWIFT $UVW1$ and $UVW2$ filters has a quite strong red tail. If, as is often the case for SNe, there is a strong blueward slope of the spectrum in the UV region this will result in a red leakage that might even dominate the flux in these filters. This can be seen in Fig. 4 where the rise in the U filter is reflected in the $UVW1$ and $UVW2$ filters whereas the $UVM2$ filter shows a gradual decline. In Fig. 5 we quantify this by showing the fractional red leakage defined as the fractional flux more than half the equivalent width redwards the effective wavelengths of the filters. The spectrum was interpolated from the photometry as explained in Sect. 3.2 exluding the $UVW1$ and $UVW2$ filter. Around the maximum the leakage is much as 80 and 70 percent in the $UVW1$ and $UVW2$ filters respectively. Given this the $UVW1$ and $UVW2$ lightcurves does not reflect the evolution of the spectrum at their effective wavelengths and we will exclude these when calculating the bolometric lightcurve in Sect. 3.2.

3.2. Bolometric lightcurve

To calculate the pseudo-bolometric lighturve of SN 2011dh we have used a combination of two diffetent methods. One for wavelength regions whith spectral information and one for wavelength regions whithour. The prefix pseudo here refers to the fact that a true bolometric lightcurve should be integrated over all wavelenghts. We do not assume anything about the flux in wavelength regions not covered by data but leave that to others.

Wavelength regions with spectral information was divided into sub-regions corresponding to each photometric band. For each epoch of photometry in each of the sub-regions a bolometric correction defined as $M_{bol,i} = M_i + BC_i$ was determined by synthetic photometry and integration of the sub-region spectral flux. The bolometric magnitude in the region was then calculated as the sum over all sub-regions. Spectra were lineary interpolated to match each epoch of photometry as described in Sect 3.3.2. This method makes use of both spectral and photometric information and is well motivated as long as the spectral sampling is good.

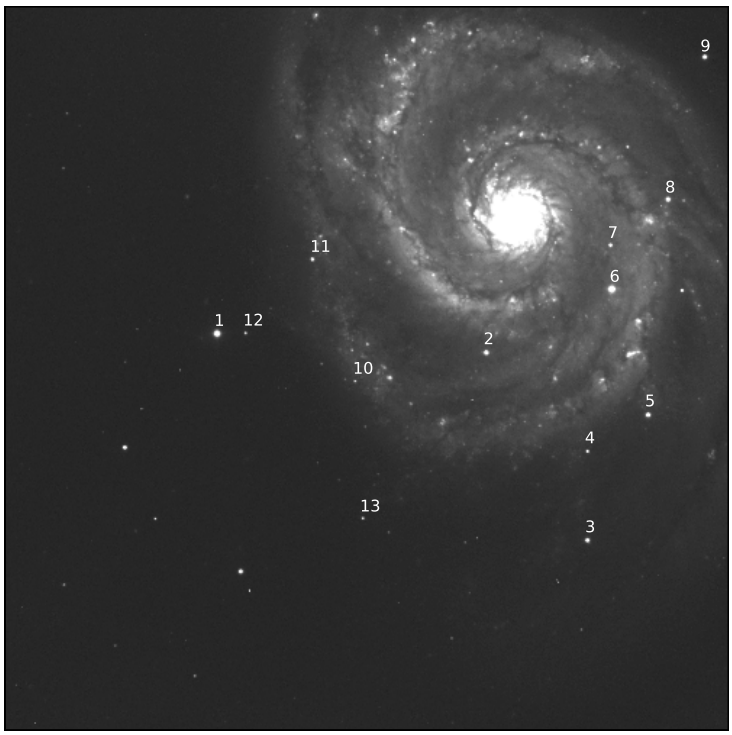

Fig. 1. Reference stars used for calibration of the optical and NIR photometry.

In wavelength regions without spectral information we have log-lineary interpolated the flux per wavelength between the effective wavelengths of the filters. This was done under the constraint that the weighted average over the filter response func-

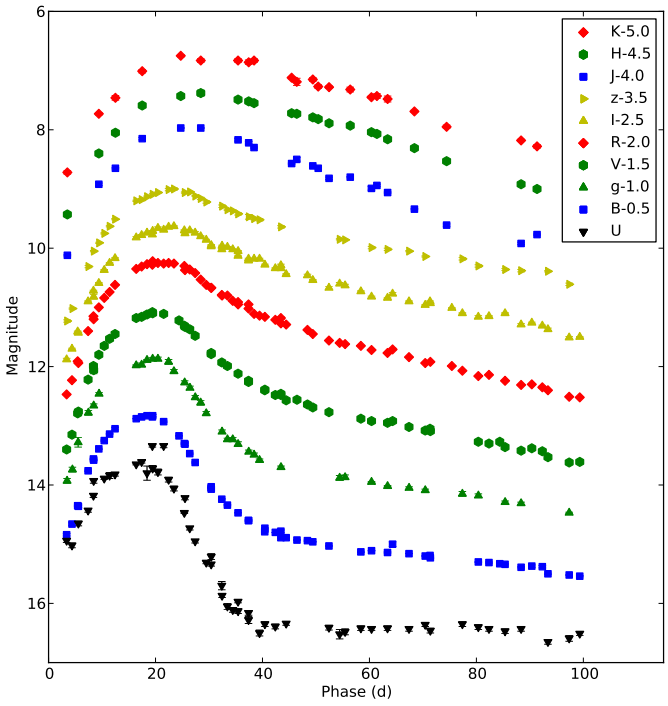

Fig. 2. Photometric evolution of SN 2011dh in the UBVRI (Johnson-Cousine), gz (Sloan) and JHK (2MASS) bands. For clarity individual bands have been shifted by the amount specified in the upper right corner.

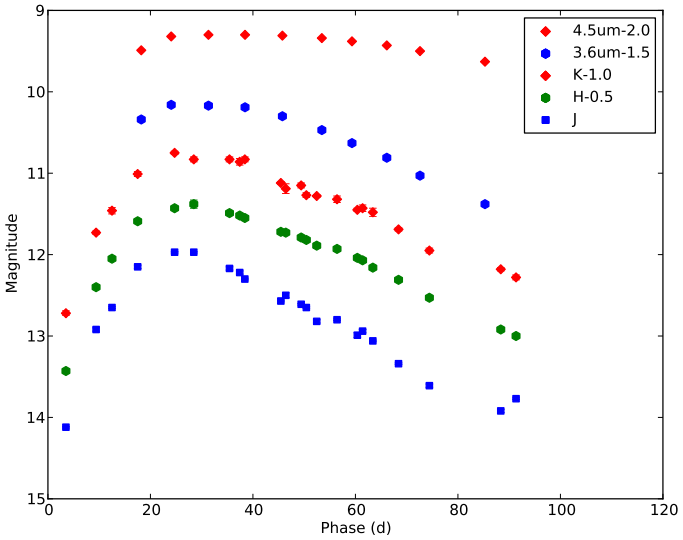

Fig. 3. Photometric evolution of SN 2011dh the Spitzer 3.6 and 4.5 micron bands and NIR between 0 and 100 days. For clarity individual bands have been shifted by the amount specified in the upper right corner.

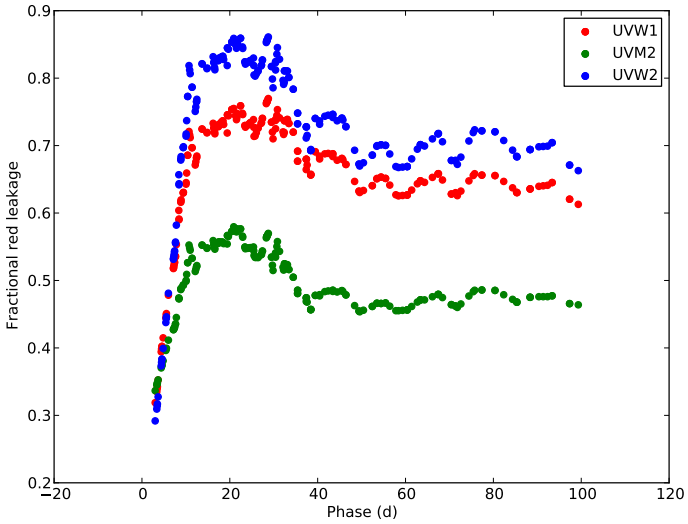

Fig. 5. Fractional red leakage in the SWIFT UVW1, UVM2 and UVW2 filters.

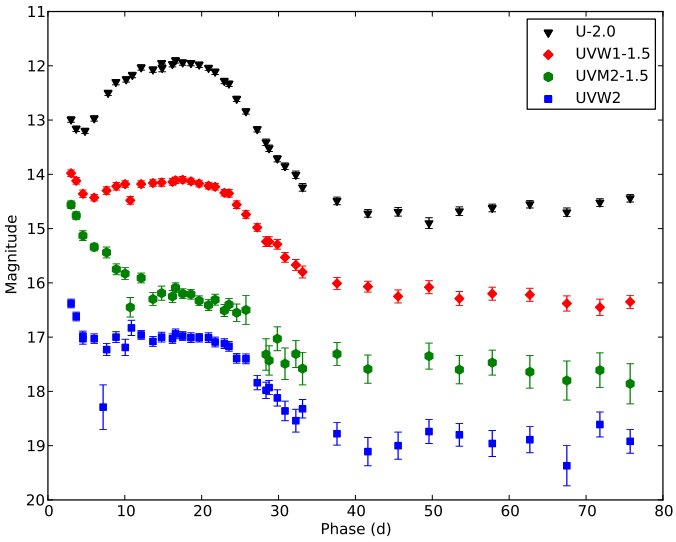

Fig. 4. Photometric evolution of SN 2011dh the SWIFT U,UVW1,UVM2 and UVW2 bands between 0 and 100 days. For clarity individual bands have been shifted by the amount specified in the upper right corner.

tions of the interpolated flux per wavelength equaled the flux per wavelength as determined by the zero points. The solution was determined by a simple iterative scheme. The total flux in the region was then calculated by integration of the interpolated flux per wavelength.

For each epoch magnitudes of missing bands were calculated by linear interpolation in magnitude of the band with most data points (if needed) followed by linear interpolation in colour of successive bands (if needed). This scheme was used as the colour evolution of SNe is usually slower than the evolution in magnitude.

Filter response functions were adopted from (Moro & Munari 2000 !Check that these are correct!, !add UV and MIR references here!) and filter zero points from (Bessell 1979, Cohen et al. 2003, !add UV and MIR references here!).

For SN 2011dh where we have optical and NIR spectra with good sampling between 3 and 100 days we have used the first method in the U-K region and the second method in the UV and MIR regions. The pseudo-bolometric UV-MIR lightcurve of SN 2011dh is shown in Fig. 6. This data together with the photosperic velocity as estimated in Sect. 3.3.2 provide the basis for hydro-dynamical modeling of the SN 2011dh presented in Bersten et al. (2012). For comparison we also show the pseudo-bolometric lightcurve calculated using the second method only. In Fig. 7 we show the fractional luminosity in the UV, optical, NIR and MIR regions respectively. The optical flux starts out at about 70 percent, increasing to about 75 percent at the maximum (20 days), decreasesing to about 60 percent at the beginning of the tail (40 days) and increasing again to about 70 percent at 100 days. The NIR flux starts out at about 20 percent, decreasing to about 15 percent around maximum (20 days), increasing to about 30 percent at the beginning of the tail and then decreasing again to about 20 percent. The UV flux starts out at about 10 percent, decreasing to the percent level at the beginning of the tail (40 days) and onwards. The MIR flux starts out at the percent level, increasing to about 5 percent at the beginning of the tail (40 days) and onwards.

!We should probably provide estimates also for the missing wavelength regions!

3.3. Spectroscopic Observations

An extensive campaign of optical and NIR spectroscopic observations was initiated for SN 2011dh shortly after discovery with data obtained from a multitude of telescopes. Data have been obtained by the NOT, the TNG, the WHT, the Calar Alto 2.2 m telescope, the Asiago 1.82m telecope and the LBT.

3.3.1. Reduction

The optical spectroscopic data were reduced, extracted and flux and wavelength calibrated with the QUBA pipeline (Stefano Valenti et al. 2011). The NIR spectroscopic data were reduced, extracted, flux and wavelength calibrated and corrected for telluric absorption with an IRAF based pipeline written in python. Details of all spectroscopic observations, the telescope and in-

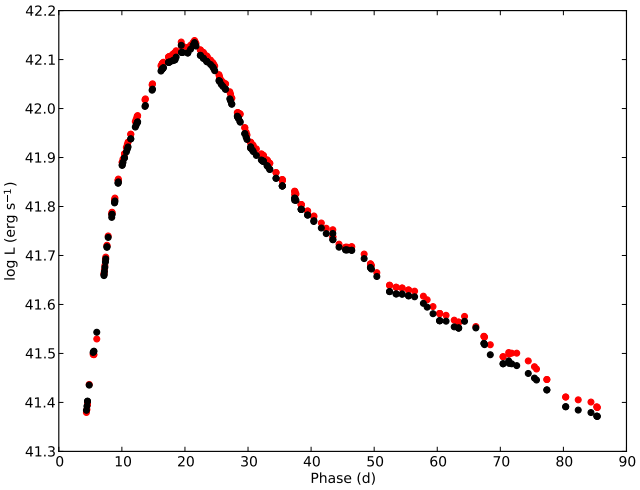

Fig. 6. Pseudo-bolometric UV-MIR lightcurve for SN 2011dh calculated from spectroscopic and photometric data. The UV-MIR lightcurve calculated from photometric data only is shown in red for comparison

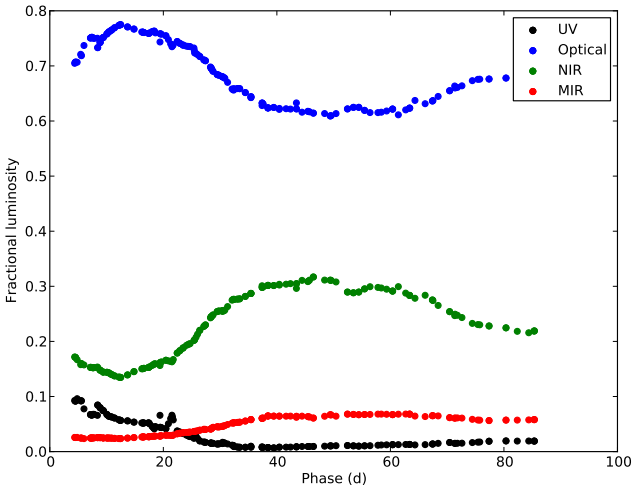

Fig. 7. Fractional UV, optical, NIR and MIR luminosity for SN 2011dh.

strument used, epoch and instrument characteristics are given in Table 13.

3.3.2. Results

All reduced, extracted and calibrated spectra are available for download in machine readable format in the online version of the paper as well as from the WISEASS database. For clarity most figures in this section will be based on time-interpolations of the spectral seqence. The interpolations have been done according to the following scheme. First all spectra were re-sampled and smoothed to a common sampling and resolution. Then, for each interpolation epoch the spectra closest in time before and after the epoch were identified resulting in one or more wavelength ranges and associated pre and and post epoch spectra. For each wavelength range the pre and post epoch spectra were then lineary interpolated and finally scaled and smoothly averaged using a 500 Å !Check this! overlap range. Spectra interpolated using this method were also used in the calculation of the bolometric lightcurve in Sect. 3.2

Fig. 8 shows the optical and NIR (interpolated) spectral evolution of SN 2011dh for day 4-88 with a 4-day sampling. Fig. 9

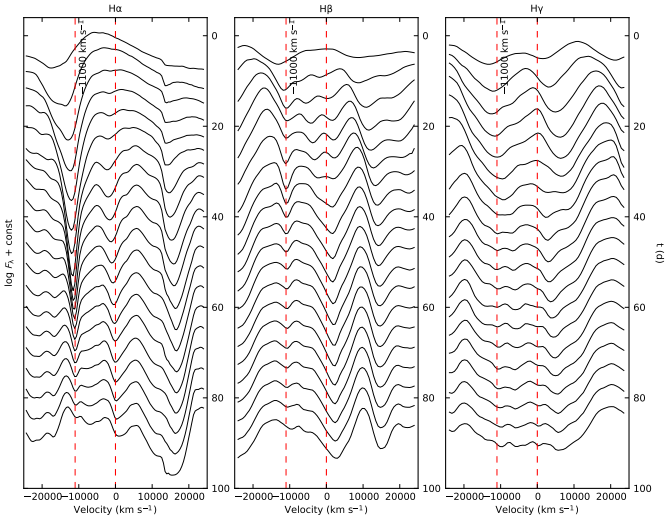

Fig. 10. Closeup of (interpolated) spectral evolution centered on the Hα (left panel), Hβ (middle panel) and the Hγ (right panel) lines. All panels also shows the -11000 km s^{-1} velocity roughly corresponding to the minimum velocity for Hα absorption. The spectra have been corrected for redshift and dereddened.

shows the optical (interpolated) spectral evolution of SN 2011dh for day 4-34 with a 2-day sampling. It's clear from these figures that the transition, common to all type IIb SNe, where the hydrogen lines fades away and Helium lines increases in strength occurs between 20 and 60 days. Fig. 10, 11 and 12 shows closeups centered on the Hα, Hβ and Hγ lines, the HeI 10830 Å, HeI 20580 Å and HeI 7067 Å lines and CaI 3933 Å, CaII 8662 Å and FeI 5169 Å lines. The minimum velocity for absorption in Hα, roughly at 11000 km s^{-1}, have been marked. These figures suggests that a transition in the ejecta from He core to H envelope material occurs at this velocity. The maximum velocity for Hα absorption in the erliest spectra suggest that the H envelope extends to at least 25000 km s^{-1}. We will discuss this further when comparing to SNe 1993J and 2008ax in Sect. 3.4. Clearly all this is just educated guesses and have to be confirmed by detailed spectral modeling. In Fig 13 we plot the absorption minimum velocities for FeI 5169 Å, HeI 7067 Å, HeI 10833 Å, HeI 20587 Å and H as determined from the (interpolated) spectral sequence. These were measured by an simple automatic centering algorithm where the spectra were first smoothed down to 1000 km s^{-1} for the He lines and 500 km s^{-1} otherwise and the absorption minimum then traced through the spectral sequence. The absorption minimum of the FeI 5169 Å line have been suggested as a good tracer of the photospheric velocity !Motivation or reference here!. This data together with the bolometric lightcurve calculated in Sect. 3.2 provides the basis for the hydrodynamical modeling presented in Bersten et al. (2012).

'

3.4. Comparison to other SNe

In this section we compare the observations of SN 2011dh to the well observed Type IIb SNe 1993J and 2008ax. SN 1993J is one of the best observed SNe ever and the nature of this SN and its progenitor star is quite well understood. Shigeyama et al. (1994) and Woosley et al. (1994) used hydrodynamical modeling to show that a progenitor star with an initial mass of 12-15 $M_\odot$ with an extended (?-? $R_\odot$) but low mass (0.2-0.9

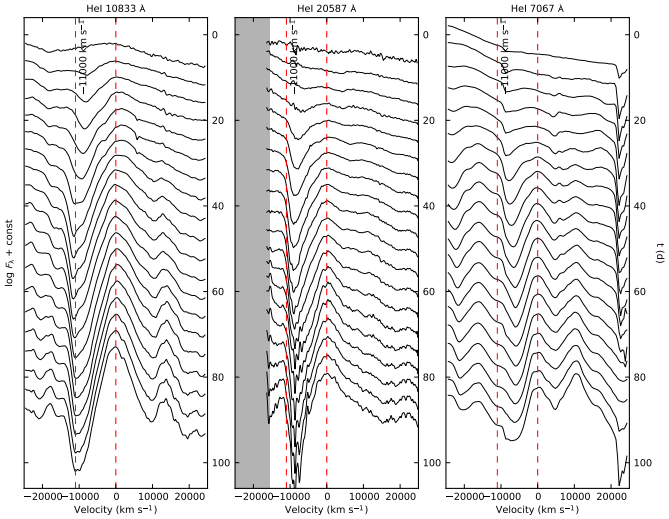

Fig. 11. Closeup of (interpolated) spectral evolution centered of the HeI 10833 Å (left panel), HeI 20587 Å (middle panel) and the HeI 7067 Å (right panel) lines. All panels also shows the -11000 km s^{-1} velocity roughly corresponding to the minimum velocity for Hα absorption. The spectra have been corrected for redshift and dereddened.

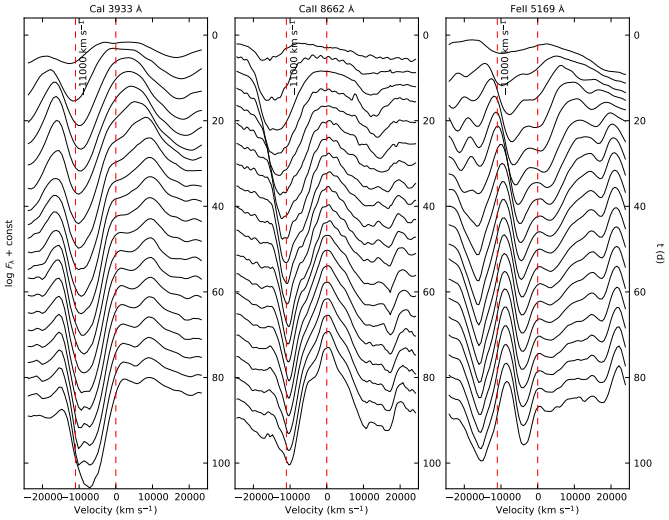

Fig. 12. Closeup of (interpolated) spectral evolution centered of the CaI 3933 Å (left panel), CaII 8662 Å (middle panel) and the FeI 5169 Å (right panel) lines. All panels also shows the -11000 km s^{-1} velocity roughly corresponding to the minimum velocity for Hα absorption. The spectra have been corrected for redshift and dereddened.

$M_\odot$) hydrogen envelope well reproduce the observed bolometric ligtcurve. This was later confirmed by the more detailed modeling of Blinnikov et al. (1998). !Describe results from spectral modeling here! !Describe results from progenitor observations here! For the comparisons photometric and spectroscopic data for SN 1993J were taken from Lewis et al. (1994) and !reference for JHK photometry data here!. Distance and extinction have been adopted from Lewis et al. (1994). SN 2008ax is another well observed Type IIb SN but the nature of this SN and it's progenitor star is not as well understood as for 1993J. Tsvetkov et al. (2009) has however used the hydrodynamical code STELLA (Blinnikov et al. 1998 !Is this reference correct!) to show that a progenitor star with an initial mass of 13 $M_\odot$ with an extended (600 $R_\odot$) and low mass (not specified) hydrogen envelope well reproduce the UBVRI lightcurves except for the first few days. !Describe results from progenitor observations here! Photometric and spectroscopic data for SN 2008ax were taken from Pastorello et al. (2008), Roming et al. (2009), Tsvetkov et al. (2009) and Taubenberger et al. (2011) !Check that this is true also for the spectra!.

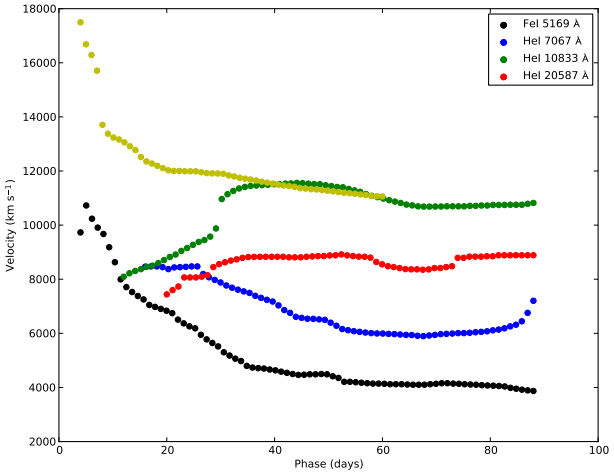

Fig. 13. Velocity evolution of the absorption minimum of the FeI 5169 Å, HeI 7067 Å, HeI 10833 Å, HeI 20587 Å and H lines as automaticly measured from the (interpolated) spectral sequence.

In Fig. 14 we show the pseudo-bolometric $U-K$ lightcurves of SNe 2011dh, 1993J and 2008ax as calculated with the second method in Sect. 3.2. Except for the first few days the shape is very similar. As is clear from the modeling of both 1993J (see above) and 2011dh (Bersten et al. 2012) the differences during the first few days of evolution could be explained by differences in radius and mass of the hydrogen envelope. SN 2011dh is significanly fainter than SNe 1993J and 2008ax though suggesting a smaller mass of ejected ^{56}Ni powering the lightcurve which is also confirmed by the hydrodynamical modeling in Bersten et al. (2012). In Fig. 15 we show the colour evolution of the same SNe. Except, again, for the first few days, SN 2011dh is significantly redder than SNe 1993J and 2008ax. The cause of this could be an intrinsic colour difference or host galaxy extinction. Detailed spectral modeling is needed to discriminate between the two scenarious. As discussed in Sect. 2.2 there is no evidence for high host galaxy extinction and this is what we have assumed in this paper. It's interesting to note though that a total extinction of A_V=1 would make both the colours (see Fig. 15) and the luminosity (see Fig. 14) of the SN quite similar to SNe 1993J and 2008ax. Clearly this is an issue for further investigations.

4. Discussion

5. Conclusions

This is the conclusion section.

6. Acknowledgements

This is the aknowledgements.

Table 2. Johnson-Cousine (UBVRI) average colour constants for the different telescope/instrument combinations.

Instrument	$C_{U,UB}$	$C_{B,BV}$	$C_{V,BV}$	$C_{V,VR}$	$C_{R,VR}$	$C_{I,RI}$	$C_{I,VI}$
NOT (ALFOSC)	0.0819	-0.0209	-0.0484		-0.0636		-0.0209
LT (RATCam)	0.01	0.0153	-0.07	-0.13	-0.18	-0.17	-0.08
CA (CAFOS)	0.23	0.14	-0.03	-0.05	0.00	0.23	!Check these!
ASIAGO (Schmidt)		0.1	-0.1	-0.19	-0.21	-0.035	-0.016
WHT (ACAM)							

Table 3. Sloan (ugriz) average colour constants for the different telescope/instrument combinations.

Instrument	$C_{u,ug}$	$C_{g,gr}$	$C_{r,gr}$	$C_{i,ri}$	$C_{z,iz}$
NOT (ALFOSC)					
LT (RATCam)	0.055	0.151	0.055	0.123	0.105

Table 4. 2MASS (JHK) average colour constants for the different telescope/instrument combinations.

Instrument	$C_{J,JH}$	$C_{H,JH}$	$C_{K,HK}$	$C_{K,JK}$
NOT (NOTCAM) TNG (NICS)				
TCS (CAIN)				
WHT (LIRIS)				
CA (O2000)				

Table 5. UBVRI (Johnson-Cousine) magnitudes of local reference stars used to calibrate the photometry.

id	RA	DEC	*U*	*B*	*V*	*R*	*I*
1	$13^h\ 30^m\ 14.9^s$	47 deg 10 27″	14.617	14.317	13.601	13.188	12.815
2	$13^h\ 29^m\ 55.4^s$	47 deg 10 05″	17.766	16.343	15.107	14.334	13.681
3	$13^h\ 29^m\ 48.6^s$	47 deg 07 42″	16.147	16.235	15.659	15.228	14.915
4	$13^h\ 29^m\ 48.3^s$	47 deg 08 48″	18.881	18.254	17.362	16.750	16.281
5	$13^h\ 29^m\ 43.8^s$	47 deg 09 14″	15.511	15.848	15.394	15.049	14.744
6	$13^h\ 29^m\ 46.0^s$	47 deg 10 47″	14.120	14.007	13.433	13.061	12.726
7	$13^h\ 29^m\ 46.0^s$	47 deg 11 20″	17.186	17.149	16.667	16.292	15.941
8	$13^h\ 29^m\ 41.6^s$	47 deg 11 52″	15.757	15.773	15.244	14.853	14.517
9	$13^h\ 29^m\ 38.6^s$	47 deg 13 36″	16.743	16.197	15.285	14.746	14.198

Table 6. ugriz (Sloan) magnitudes of local reference stars used to calibrate the photometry.

id	RA	DEC	*u*	*g*	*r*	*i*	*z*
1	$13^h\ 30^m\ 14.9^s$	47 deg 10 27″	15.461	13.871	13.404	13.296	13.220
2	$13^h\ 29^m\ 55.4^s$	47 deg 10 05″	18.327	15.674	14.572	14.162	13.933
3	$13^h\ 29^m\ 48.6^s$	47 deg 07 42″	16.871	15.790	15.335	15.317	15.147
4	$13^h\ 29^m\ 48.3^s$	47 deg 08 48″	19.543	17.779	16.903	16.679	16.502
5	$13^h\ 29^m\ 43.8^s$	47 deg 09 14″	16.291	15.497	15.188	15.113	15.078
6	$13^h\ 29^m\ 46.0^s$	47 deg 10 47″	14.765	13.608	13.151	13.089	13.016
10	$13^h\ 30^m\ 5.0^s$	47 deg 09 47″	18.475	18.860	17.520	16.815	16.440
11	$13^h\ 30^m\ 7.7^s$	47 deg 11 19″	18.419	16.809	16.296	16.087	15.941
12	$13^h\ 30^m\ 12.8^s$	47 deg 10 27″	18.993	18.277	17.556	17.240	17.053
13	$13^h\ 30^m\ 4.9^s$	47 deg 08 05″	19.288	18.491	17.227	16.160	15.599

Table 7. JHK (2MASS) magnitudes of local reference stars used to calibrate the photometry.

id	RA	DEC	J	H	K
1	$13^h\ 30^m\ 14.9^s$	47 deg 10 27″	12.373	12.021	11.983
2	$13^h\ 29^m\ 55.4^s$	47 deg 10 05″	12.846	12.248	12.142
3	$13^h\ 29^m\ 48.6^s$	47 deg 07 42″	14.373	14.010	13.962
4	$13^h\ 29^m\ 48.3^s$	47 deg 08 48″	15.463	15.000	15.062
5	$13^h\ 29^m\ 43.8^s$	47 deg 09 14″	14.284	13.976	13.912
6	$13^h\ 29^m\ 46.0^s$	47 deg 10 47″	12.261	11.975	11.941
10	$13^h\ 30^m\ 5.0^s$	47 deg 09 47″	15.324	14.689	14.504
11	$13^h\ 30^m\ 7.7^s$	47 deg 11 19″	15.033	14.627	14.634
12	$13^h\ 30^m\ 12.8^s$	47 deg 10 27″	16.036	15.686	15.723
13	$13^h\ 30^m\ 4.9^s$	47 deg 08 05″	14.319	13.607	13.383

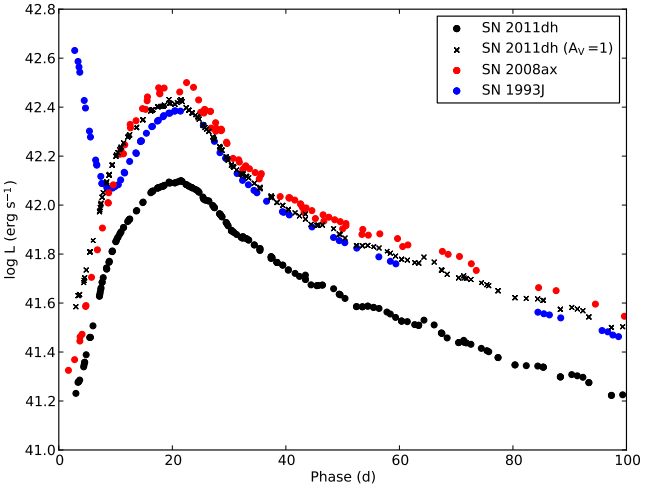

Fig. 14. Pseudo-bolometric $U - K$ lightcurve for SN 2011dh as compared to SNe 1993J and 2008ax.

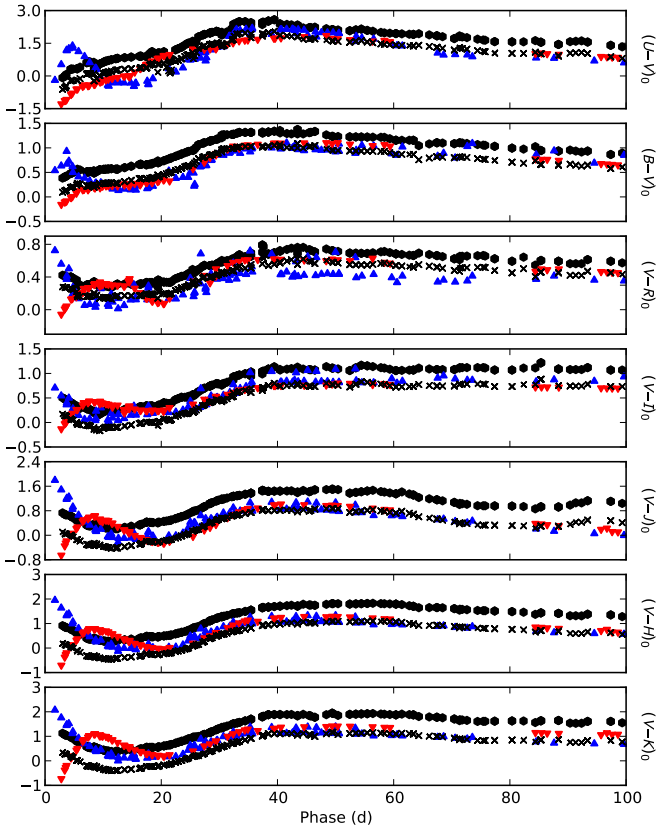

Fig. 15. Colour evolution of SN 2011dh as compared to SNe 1993J and 2008ax.

References

Arcavi I. et al., 2011, ApJ, 742, L18
Baron E. et al., 1996, MNRAS, 279, 799
Baron E. et al., 2007, ApJ, 662, 1148
Bersten M. et al., 2012, in preparation
Bessel M. S., 1979, PASP, 91, 589
Bietenholz M. et al., 2012, ArXiv, 1201.0771
Blinnikov S. et al., 1998, ApJ, 496, 454
Cardelli, J. A., Clayton, G. C., & Mathis, J. S. 1989, ApJ, 345, 245
Ciardullo R. et al., 2002, ApJ, 577, 31
Cohen M., Wheaton W. A., Megeath S. T., 2003, AJ, 126, 1090
Crocket R. et al., 2008, MNRAS, 391, 5L
Dessart L. et al., 2008, ApJ, 675, 644
Van Dyk S. D. et al., 2011, ApJ, 741, L28
Feldmeier J. J. et al, 1997, ApJ, 479, 231
Georgiev T. B. et al., 1990, AZh, 16, 979
Iwamoto K. et al., 1994, ApJ, 437, L115
Krauss M. et al., 2012, ApJ, 750, 40
Lewis J. et al., 1994, MNRAS, 266, 27L
Marti-Vidal I. et al, 2011, A&A, 535, L10
Maund J. et al., 2011, ApJ, 739, L37
Moro D., Munari U., 2000, A%AS, 147, 361
Munari U., Zwitter T., 1997, A&A, 318, 269
Murphy J. et al., 2011, ApJ, 742, L4
Pastorello A. et al., 2008, MNRAS, 389, 955
Pastorello A., Valenti S., Zampieri L. et al., 2009, MNRAS, 394, 2266
Poznanski D. et al., 2009, ApJ, 694, 1067
Reiland, T., Griga, T., & Riou, A. et al. 2011, CBET, 2736, 1
Ritchey A. et al., 2012, ApJ, 748, 11
Roming P. et al., 2009, ApJ, 704, L118
Schlegel D. J., Finkbeiner D. P., Davis M., ApJ, 500, 525
Shigeyama T. et al., 1994, ApJ, 420, 341
Smartt S.J., Eldridge J.J., Crockett R.M., Maund J.R., 2009, MNRAS, 395, 140
Skrutskie M. F. et al., 2006, AJ, 131, 1163
Soderberg A. et al., 2011, ArXiv, 1107.1876
Szczygiel D. et al., 2012, ApJ, 747, 23
Takats K., Vinko J., 2006, MNRAS 372, 1735
Taubenberger S., 2011, MNRAS, 413, 2140
Tonry J. L. et al., ApJ, 546, 681
Tsvetkov D. et al., 2009, PZ, 29, 2
Valenti S. et al., 2011, MNRAS, 416, 3138
Vinko J. et al., 2012, A&A, 540, 93
Woosley S. et al., 1994, ApJ, 429, 300

Table 8. Optical Johnsson-Cousine (UBVRI) magnitudes for SN 2011dh.

JD (+2400000)	Phase (d)	*U*	*B*	*V*	*R*	*I*	Instrument
55716.38	3.38	14.94 (0.03)	15.34 (0.02)	14.90 (0.01)	14.47 (0.01)	14.38 (0.02)	LT (RATCam)
55717.38	4.38	15.02 (0.04)	15.16 (0.02)	14.65 (0.02)	14.23 (0.01)	14.20 (0.01)	LT (RATCam)
55718.44	5.44		14.85 (0.01)	14.29 (0.01)	13.91 (0.01)	13.91 (0.01)	LT (RATCam)
55718.57	5.57	14.65 (0.04)	14.86 (0.02)	14.26 (0.02)	13.94 (0.01)	13.93 (0.01)	CA (CAFOS)
55720.39	7.39	14.43 (0.03)	14.26 (0.01)	13.72 (0.02)	13.40 (0.01)	13.40 (0.01)	LT (RATCam)
55721.39	8.39	14.18 (0.03)	14.06 (0.01)	13.49 (0.01)	13.15 (0.01)	13.22 (0.01)	LT (RATCam)
55721.43	8.43	13.93 (0.04)	14.08 (0.00)	13.56 (0.06)	13.20 (0.01)	13.32 (0.04)	NOT (ALFOSC)
55722.40	9.40		13.89 (0.01)	13.30 (0.01)	13.00 (0.01)	13.09 (0.01)	LT (RATCam)
55723.41	10.41	13.89 (0.02)	13.75 (0.01)	13.15 (0.01)	12.84 (0.01)	12.87 (0.01)	LT (RATCam)
55724.41	11.41	13.84 (0.05)	13.64 (0.01)	13.03 (0.01)	12.74 (0.01)	12.75 (0.01)	LT (RATCam)
55725.43	12.43	13.82 (0.03)	13.55 (0.02)	12.95 (0.02)	12.62 (0.01)	12.67 (0.01)	LT (RATCam)
55729.39	16.39	13.65 (0.01)	13.38 (0.00)	12.68 (0.03)	12.35 (0.01)	12.32 (0.02)	LT (RATCam)
55730.40	17.40	13.61 (0.02)	13.35 (0.01)	12.66 (0.01)	12.31 (0.01)	12.28 (0.01)	LT (RATCam)
55731.41	18.41	13.80 (0.12)	13.33 (0.00)	12.62 (0.02)	12.27 (0.01)	12.24 (0.01)	LT (RATCam)
55732.41	19.41	13.34 (0.02)	13.35 (0.00)	12.58 (0.01)	12.28 (0.00)	12.27 (0.03)	NOT (ALFOSC)
55732.46	19.46	13.72 (0.05)	13.33 (0.02)	12.60 (0.01)	12.22 (0.01)	12.21 (0.01)	LT (RATCam)
55733.45	20.45	13.78 (0.05)			12.25 (0.01)	12.16 (0.02)	LT (RATCam)
55734.52	21.52	13.34 (0.03)	13.43 (0.01)	12.61 (0.01)	12.26 (0.01)	12.19 (0.01)	CA (CAFOS)
55735.45	22.45	13.91 (0.04)			12.25 (0.01)	12.14 (0.01)	LT (RATCam)
55736.44	23.44	14.06 (0.04)			12.26 (0.01)	12.13 (0.01)	LT (RATCam)
55737.39	24.39		13.67 (0.00)	12.72 (0.01)			LT (RATCam)
55738.39	25.39	14.47 (0.01)	13.80 (0.01)	12.81 (0.01)	12.30 (0.01)	12.20 (0.01)	LT (RATCam)
55738.51	25.51	14.22 (0.03)	13.81 (0.02)	12.83 (0.01)	12.37 (0.01)	12.25 (0.01)	NOT (ALFOSC)
55739.40	26.40	14.73 (0.03)	13.97 (0.01)	12.87 (0.02)	12.36 (0.01)	12.20 (0.01)	LT (RATCam)
55740.41	27.41	14.95 (0.03)	14.12 (0.01)	12.98 (0.01)	12.42 (0.01)	12.24 (0.02)	LT (RATCam)
55741.44	28.44				12.53 (0.00)	12.30 (0.01)	LT (RATCam)
55742.49	29.49	15.31 (0.02)			12.62 (0.01)	12.36 (0.01)	LT (RATCam)
55743.41	30.41	15.34 (0.03)	14.53 (0.01)	13.29 (0.02)	12.67 (0.00)	12.47 (0.02)	NOT (ALFOSC)
55743.41	30.41		14.55 (0.01)	13.27 (0.02)			LT (RATCam)
55743.42	30.42	15.21 (0.05)	14.57 (0.02)		12.67 (0.01)	12.45 (0.01)	CA (CAFOS)
55745.39	32.39	15.70 (0.07)	14.74 (0.01)	13.43 (0.00)	12.79 (0.01)	12.52 (0.01)	NOT (ALFOSC)
55745.44	32.44	15.87 (0.03)			12.80 (0.01)	12.46 (0.01)	LT (RATCam)
55746.44	33.44	16.05 (0.05)	14.84 (0.01)	13.49 (0.01)	12.80 (0.01)	12.48 (0.01)	LT (RATCam)
55747.44	34.44	16.11 (0.04)			12.89 (0.01)	12.52 (0.01)	LT (RATCam)
55748.43	35.43	15.97 (0.02)	14.97 (0.00)	13.62 (0.01)	12.91 (0.00)	12.63 (0.01)	NOT (ALFOSC)
55748.44	35.44	16.13 (0.04)			12.95 (0.01)	12.55 (0.01)	LT (RATCam)
55750.39	37.39	16.16 (0.04)	15.10 (0.01)	13.74 (0.01)	13.02 (0.01)	12.71 (0.01)	NOT (ALFOSC)
55750.39	37.39	16.28 (0.06)	15.10 (0.01)	13.76 (0.01)	12.95 (0.01)	12.68 (0.01)	LT (RATCam)
55751.43	38.43				13.11 (0.01)	12.68 (0.01)	LT (RATCam)
55752.45	39.45	16.50 (0.05)			13.14 (0.01)	12.68 (0.01)	LT (RATCam)
55753.42	40.42		15.29 (0.01)	13.90 (0.01)			LT (RATCam)
55753.45	40.45	16.35 (0.04)	15.23 (0.01)	13.89 (0.01)	13.16 (0.01)	12.78 (0.01)	NOT (ALFOSC)
55755.40	42.40	16.39 (0.04)	15.30 (0.00)	13.98 (0.01)	13.21 (0.00)	12.84 (0.01)	NOT (ALFOSC)
55756.44	43.44		15.28 (0.02)	13.96 (0.02)	13.18 (0.02)	12.79 (0.02)	ASIAGO (SCHMIDT)
55756.44	43.44		15.39 (0.01)	13.98 (0.02)	13.27 (0.01)	12.84 (0.01)	LT (RATCam)
55757.43	44.43	16.34 (0.03)	15.39 (0.01)	14.07 (0.02)	13.29 (0.01)	12.94 (0.01)	NOT (ALFOSC)
55759.45	46.45		15.43 (0.01)	14.06 (0.02)			LT (RATCam)
55761.41	48.41		15.44 (0.01)	14.14 (0.01)	13.38 (0.01)	12.96 (0.02)	ASIAGO (SCHMIDT)
55762.41	49.41		15.46 (0.00)	14.19 (0.02)	13.45 (0.01)	13.04 (0.01)	NOT (ALFOSC)
55765.43	52.43	16.41 (0.04)	15.53 (0.00)	14.27 (0.02)	13.56 (0.01)	13.17 (0.02)	NOT (ALFOSC)
55767.43	54.43	16.52 (0.08)			13.60 (0.01)	13.10 (0.02)	LT (RATCam)
55768.45	55.45	16.48 (0.05)			13.62 (0.01)	13.13 (0.02)	LT (RATCam)
55771.40	58.40	16.42 (0.04)	15.63 (0.01)	14.38 (0.01)	13.65 (0.01)	13.23 (0.01)	CA (CAFOS)
55773.39	60.39	16.43 (0.03)	15.61 (0.00)	14.42 (0.01)	13.72 (0.01)	13.32 (0.01)	NOT (ALFOSC)
55776.38	63.38	16.42 (0.04)	15.64 (0.01)	14.45 (0.02)	13.77 (0.00)	13.34 (0.01)	NOT (ALFOSC)
55777.33	64.33		15.50 (0.04)	14.42 (0.01)	13.71 (0.02)	13.27 (0.02)	ASIAGO (SCHMIDT)
55780.40	67.40	16.43 (0.04)	15.66 (0.00)	14.52 (0.01)	13.84 (0.00)	13.40 (0.01)	NOT (ALFOSC)
55783.43	70.43	16.36 (0.03)	15.70 (0.01)	14.58 (0.01)	13.94 (0.01)	13.46 (0.01)	NOT (ALFOSC)
55784.33	71.33		15.69 (0.02)	14.55 (0.01)		13.40 (0.01)	ASIAGO (SCHMIDT)
55784.39	71.39	16.46 (0.04)	15.73 (0.01)	14.59 (0.01)	13.92 (0.01)	13.43 (0.01)	CA (CAFOS)
55788.41	75.41				13.99 (0.01)	13.51 (0.01)	ASIAGO (SCHMIDT)
55790.38	77.38	16.35 (0.04)			14.07 (0.01)	13.60 (0.01)	LT (RATCam)
55793.36	80.36	16.40 (0.04)	15.80 (0.01)	14.77 (0.01)	14.16 (0.01)	13.66 (0.02)	NOT (ALFOSC)
55795.35	82.35	16.43 (0.04)	15.81 (0.01)	14.80 (0.01)	14.14 (0.01)	13.65 (0.01)	CA (CAFOS)
55797.37	84.37		15.83 (0.02)	14.77 (0.01)			ASIAGO (SCHMIDT)
55798.36	85.36	16.47 (0.04)	15.84 (0.01)	14.86 (0.01)	14.24 (0.01)	13.60 (0.01)	NOT (ALFOSC)
55801.36	88.36	16.43 (0.04)	15.89 (0.01)	14.92 (0.01)	14.31 (0.01)	13.79 (0.02)	NOT (ALFOSC)
55803.36	90.36		15.87 (0.02)	14.88 (0.01)	14.30 (0.01)	13.76 (0.01)	ASIAGO (SCHMIDT)
55805.33	92.33		15.88 (0.02)	14.93 (0.02)	14.35 (0.02)	13.81 (0.01)	ASIAGO (SCHMIDT)
55806.38	93.38	16.65 (0.04)	16.00 (0.01)	15.03 (0.02)	14.40 (0.00)	13.87 (0.02)	WHT (ACAM)
55810.35	97.35	16.59 (0.05)	16.02 (0.01)	15.12 (0.02)	14.51 (0.01)	14.01 (0.02)	NOT (ALFOSC)
55812.33	99.33	16.51 (0.03)	16.04 (0.01)	15.11 (0.01)	14.52 (0.01)	14.00 (0.01)	CA (CAFOS)

Table 9. Optical Sloan (gz) magnitudes for SN 2011dh.

JD (+2400000)	Phase (d)	*g*	*z*	Instrument
55716.46	3.46	14.93 (0.04)	14.73 (0.02)	LT (RATCam)
55717.46	4.46	14.74 (0.04)	14.52 (0.01)	LT (RATCam)
55718.53	5.53	14.28 (0.08)		LT (RATCam)
55720.44	7.44	13.78 (0.04)	13.81 (0.02)	LT (RATCam)
55721.44	8.44	13.66 (0.03)	13.55 (0.01)	LT (RATCam)
55722.44	9.44	13.46 (0.02)	13.41 (0.01)	LT (RATCam)
55723.41	10.41		13.25 (0.01)	LT (RATCam)
55724.41	11.41		13.13 (0.01)	LT (RATCam)
55725.43	12.43		13.01 (0.01)	LT (RATCam)
55729.39	16.39	12.98 (0.01)	12.70 (0.01)	LT (RATCam)
55730.40	17.40	12.97 (0.03)	12.68 (0.02)	LT (RATCam)
55731.41	18.41	12.89 (0.01)	12.63 (0.01)	LT (RATCam)
55732.46	19.46	12.87 (0.02)	12.59 (0.01)	LT (RATCam)
55733.45	20.45	12.87 (0.03)	12.56 (0.01)	LT (RATCam)
55735.44	22.44	12.92 (0.04)	12.51 (0.02)	LT (RATCam)
55736.44	23.44	13.08 (0.03)	12.50 (0.02)	LT (RATCam)
55738.45	25.45	13.27 (0.03)	12.56 (0.01)	LT (RATCam)
55739.44	26.44	13.36 (0.03)	12.55 (0.01)	LT (RATCam)
55740.43	27.43	13.52 (0.03)	12.62 (0.01)	LT (RATCam)
55741.44	28.44	13.61 (0.04)	12.66 (0.02)	LT (RATCam)
55742.49	29.49	13.79 (0.03)	12.72 (0.02)	LT (RATCam)
55745.44	32.44	14.10 (0.03)	12.79 (0.02)	LT (RATCam)
55746.45	33.45	14.23 (0.02)	12.85 (0.01)	LT (RATCam)
55747.44	34.44	14.23 (0.03)	12.87 (0.01)	LT (RATCam)
55748.44	35.44	14.31 (0.04)	12.92 (0.02)	LT (RATCam)
55750.43	37.43	14.44 (0.03)	12.97 (0.04)	LT (RATCam)
55751.43	38.43	14.49 (0.03)	13.00 (0.02)	LT (RATCam)
55752.45	39.45	14.58 (0.02)	13.02 (0.02)	LT (RATCam)
55756.46	43.46	14.70 (0.02)	13.14 (0.02)	LT (RATCam)
55767.43	54.43	14.88 (0.04)	13.35 (0.01)	LT (RATCam)
55768.45	55.45	14.87 (0.04)	13.36 (0.01)	LT (RATCam)
55773.39	60.39	14.95 (0.01)	13.49 (0.02)	NOT (ALFOSC)
55776.39	63.39	15.02 (0.01)	13.52 (0.02)	NOT (ALFOSC)
55780.41	67.41	15.05 (0.02)	13.55 (0.01)	NOT (ALFOSC)
55783.44	70.44	15.09 (0.02)	13.64 (0.01)	NOT (ALFOSC)
55790.38	77.38	15.15 (0.04)	13.68 (0.02)	LT (RATCam)
55793.37	80.37	15.18 (0.03)	13.80 (0.02)	NOT (ALFOSC)
55798.37	85.37	15.29 (0.02)	13.86 (0.02)	NOT (ALFOSC)
55801.36	88.36	15.31 (0.02)	13.88 (0.02)	NOT (ALFOSC)
55806.37	93.37		13.89 (0.01)	WHT (ACAM)
55810.35	97.35	15.47 (0.01)	14.11 (0.02)	NOT (ALFOSC)

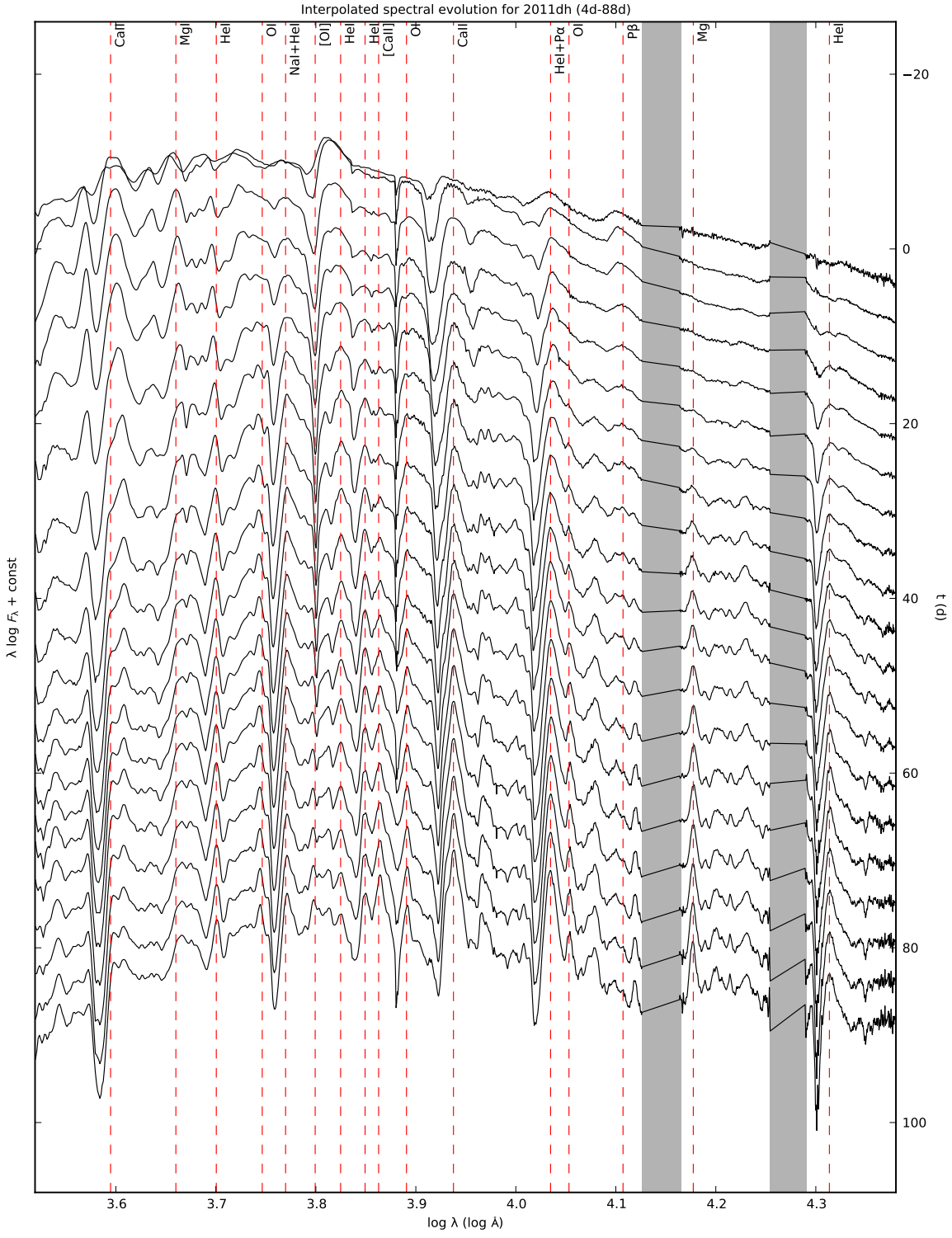

Fig. 8. Optical and NIR (interpolated) spectral evolution for SN 2011dh for day 4-88 with a 4-day sampling. To visulize the evolution the spectra in this and the following figures have been aligned to the time axis at the right border of the panel. The spectra have been corrected for redshift and dereddened. Telluric features are indicated with a ⊕ symbol.

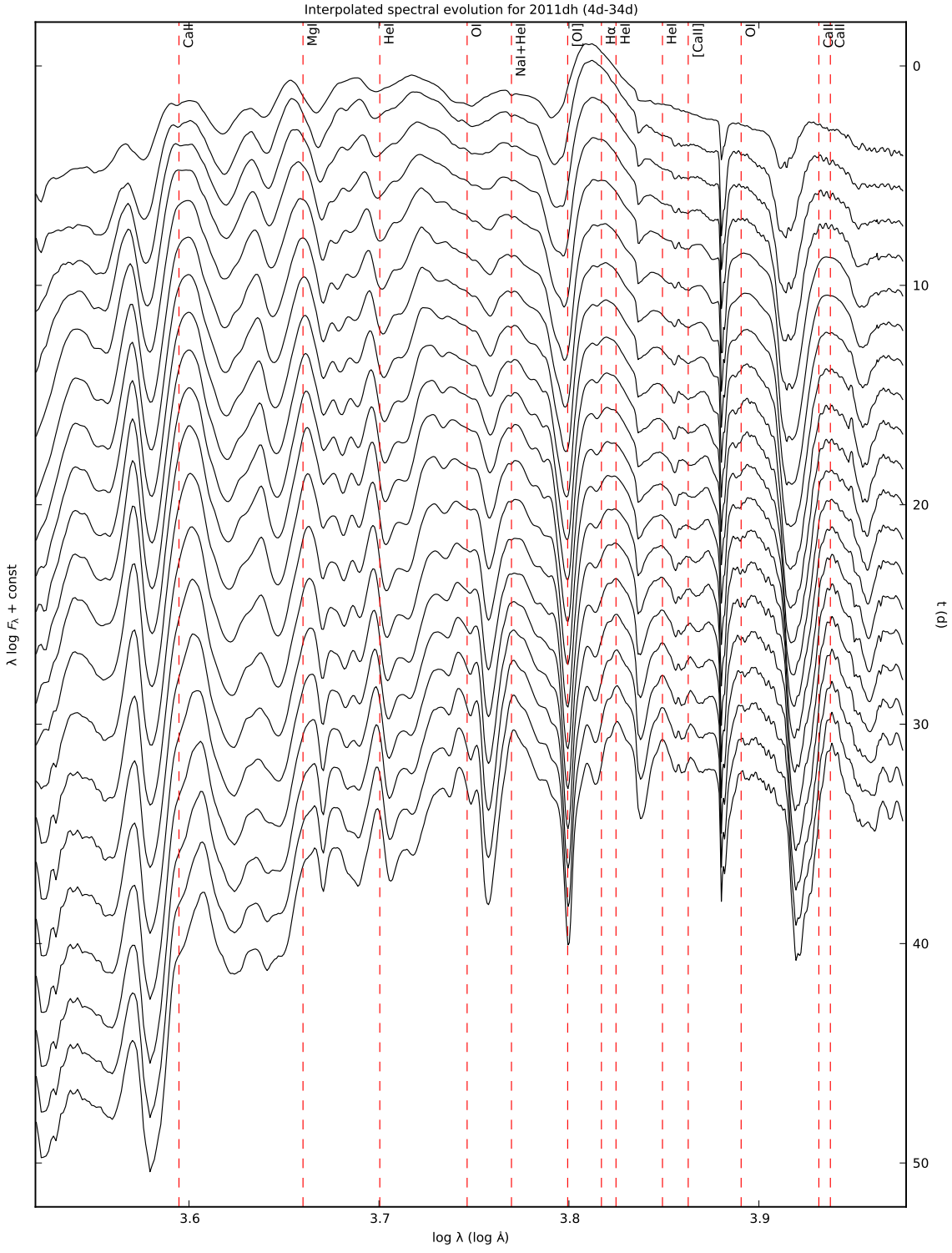

Fig. 9. Optical (interpolated) spectral evolution for SN 2011dh for day 4-34 with a 2-day sampling. The spectra have been corrected for redshift and dereddened. Telluric features are indicated with a ⊕ symbol.

Table 10. NIR 2MASS magnitudes (JHK) for SN 2011dh.

JD (+2400000)	Phase (d)	*J*	*H*	*K*	Instrument
55716.51	3.51	14.12 (0.01)	13.93 (0.01)	13.72 (0.03)	TNG (NICS)
55722.40	9.40	12.92 (0.02)	12.90 (0.01)	12.73 (0.02)	TNG (NICS)
55725.50	12.50	12.65 (0.01)	12.55 (0.02)	12.46 (0.04)	NOT (ALFOSC)
55730.51	17.51	12.15 (0.02)	12.09 (0.01)	12.01 (0.03)	TNG (NICS)
55737.72	24.72	11.97 (0.01)	11.93 (0.01)	11.75 (0.02)	LBT (LUCIFER)
55741.46	28.46	11.97 (0.01)	11.88 (0.05)	11.83 (0.03)	TCS (CAIN)
55748.43	35.43	12.17 (0.02)	11.99 (0.02)	11.83 (0.03)	TCS (CAIN)
55750.42	37.42	12.22 (0.02)	12.02 (0.02)	11.86 (0.04)	TCS (CAIN)
55751.42	38.42	12.30 (0.01)	12.05 (0.01)	11.83 (0.03)	TCS (CAIN)
55758.45	45.45	12.57 (0.01)	12.22 (0.01)	12.12 (0.02)	TNG (NICS)
55759.41	46.41	12.50 (0.03)	12.23 (0.02)	12.19 (0.06)	TCS (CAIN)
55762.41	49.41	12.61 (0.01)	12.29 (0.02)	12.15 (0.03)	TCS (CAIN)
55763.42	50.42	12.65 (0.01)	12.32 (0.03)	12.27 (0.03)	TCS (CAIN)
55765.45	52.45	12.82 (0.02)	12.39 (0.03)	12.28 (0.02)	TNG (NICS)
55769.41	56.41	12.80 (0.01)	12.43 (0.03)	12.32 (0.04)	TCS (CAIN)
55773.37	60.37	12.99 (0.03)	12.54 (0.02)	12.45 (0.02)	TNG (NICS)
55774.40	61.40	12.94 (0.02)	12.57 (0.02)	12.43 (0.04)	TCS (CAIN)
55776.40	63.40	13.06 (0.01)	12.66 (0.01)	12.48 (0.05)	TCS (CAIN)
55781.41	68.41	13.34 (0.01)	12.81 (0.02)	12.69 (0.02)	WHT (LIRIS)
55787.43	74.43	13.61 (0.02)	13.03 (0.02)	12.95 (0.03)	NOT (ALFOSC)
55801.36	88.36	13.92 (0.02)	13.42 (0.02)	13.18 (0.02)	TNG (NICS)
55804.34	91.34	13.77 (0.01)	13.50 (0.01)	13.28 (0.03)	CA (O2000)

Table 11. MIR Spitzer magnitudes (3.6μm,4.5μm) for SN 2011dh.

JD (+2400000)	Phase (d)	3.6*um*	4.5*um*	Instrument
55731.21	18.21	11.84 (0.00)	11.49 (0.00)	SPITZER (IRAC)
55737.06	24.06	11.66 (0.00)	11.32 (0.00)	SPITZER (IRAC)
55744.32	31.32	11.67 (0.00)	11.30 (0.00)	SPITZER (IRAC)
55751.46	38.46	11.69 (0.00)	11.30 (0.00)	SPITZER (IRAC)
55758.75	45.75	11.80 (0.00)	11.31 (0.00)	SPITZER (IRAC)
55766.45	53.45	11.97 (0.00)	11.34 (0.00)	SPITZER (IRAC)
55772.33	59.33	12.13 (0.00)	11.38 (0.00)	SPITZER (IRAC)
55779.12	66.12	12.31 (0.00)	11.43 (0.00)	SPITZER (IRAC)
55785.60	72.60	12.53 (0.00)	11.50 (0.00)	SPITZER (IRAC)
55798.28	85.28	12.88 (0.00)	11.63 (0.00)	SPITZER (IRAC)

Table 12. UV SWIFT magnitudes (U,UVW1,UVM2,UVW2) for SN 2011dh.

JD (+2400000)	Phase (d)	U	$UVW1$	$UVM2$	$UVW2$	Instrument
55716.01	3.01	14.99 (0.05)	15.48 (0.06)	16.06 (0.07)	16.38 (0.08)	SWIFT (UVOT)
55716.68	3.68	15.16 (0.05)	15.62 (0.06)	16.26 (0.07)	16.62 (0.08)	SWIFT (UVOT)
55717.55	4.55		15.86 (0.07)	16.63 (0.09)	16.98 (0.09)	SWIFT (UVOT)
55717.55	4.55				17.03 (0.10)	SWIFT (UVOT)
55717.82	4.82	15.20 (0.05)				SWIFT (UVOT)
55719.02	6.02	14.97 (0.05)	15.93 (0.06)	16.84 (0.07)	17.03 (0.09)	SWIFT (UVOT)
55720.18	7.18				18.29 (0.41)	SWIFT (UVOT)
55720.63	7.63		15.80 (0.07)	16.94 (0.10)		SWIFT (UVOT)
55720.64	7.64				17.23 (0.11)	SWIFT (UVOT)
55720.83	7.83	14.50 (0.05)				SWIFT (UVOT)
55721.84	8.84	14.30 (0.05)				SWIFT (UVOT)
55721.86	8.86				17.00 (0.10)	SWIFT (UVOT)
55721.90	8.90		15.72 (0.07)	17.25 (0.10)		SWIFT (UVOT)
55723.04	10.04		15.68 (0.06)	17.33 (0.11)		SWIFT (UVOT)
55723.06	10.06				17.19 (0.15)	SWIFT (UVOT)
55723.18	10.18	14.25 (0.05)				SWIFT (UVOT)
55723.71	10.71		15.98 (0.07)	17.95 (0.18)		SWIFT (UVOT)
55723.86	10.86				16.83 (0.14)	SWIFT (UVOT)
55723.98	10.98	14.17 (0.05)				SWIFT (UVOT)
55725.13	12.13	14.03 (0.05)	15.68 (0.06)	17.41 (0.09)	16.96 (0.08)	SWIFT (UVOT)
55726.66	13.66	14.07 (0.05)	15.66 (0.06)	17.80 (0.12)	17.08 (0.09)	SWIFT (UVOT)
55727.79	14.79	13.95 (0.05)	15.65 (0.07)	17.69 (0.13)	17.00 (0.09)	SWIFT (UVOT)
55727.86	14.86	14.04 (0.07)				SWIFT (UVOT)
55729.20	16.20	13.97 (0.05)	15.64 (0.06)	17.75 (0.11)	17.03 (0.09)	SWIFT (UVOT)
55729.60	16.60	13.90 (0.05)	15.61 (0.06)	17.59 (0.09)	16.94 (0.09)	SWIFT (UVOT)
55730.53	17.53	13.94 (0.05)	15.60 (0.06)	17.70 (0.09)	16.98 (0.08)	SWIFT (UVOT)
55731.60	18.60	13.95 (0.05)	15.63 (0.06)	17.71 (0.09)	17.01 (0.09)	SWIFT (UVOT)
55732.67	19.67	13.98 (0.05)	15.67 (0.06)	17.83 (0.09)	17.01 (0.08)	SWIFT (UVOT)
55733.89	20.89	14.04 (0.05)	15.71 (0.06)	17.91 (0.10)	17.01 (0.09)	SWIFT (UVOT)
55734.75	21.75	14.11 (0.05)	15.73 (0.06)	17.81 (0.10)	17.09 (0.09)	SWIFT (UVOT)
55735.95	22.95	14.28 (0.05)	15.84 (0.06)	18.01 (0.11)	17.12 (0.09)	SWIFT (UVOT)
55736.55	23.55	14.33 (0.05)	15.85 (0.07)	17.90 (0.11)	17.17 (0.09)	SWIFT (UVOT)
55737.55	24.55	14.61 (0.05)	16.06 (0.07)	18.05 (0.16)	17.39 (0.09)	SWIFT (UVOT)
55738.76	25.76	14.84 (0.05)	16.24 (0.07)	18.00 (0.27)	17.40 (0.09)	SWIFT (UVOT)
55740.23	27.23	15.17 (0.05)	16.48 (0.07)		17.84 (0.13)	SWIFT (UVOT)
55741.37	28.37	15.41 (0.06)	16.74 (0.09)	18.82 (0.29)	17.98 (0.15)	SWIFT (UVOT)
55741.77	28.77	15.52 (0.06)	16.74 (0.09)	18.93 (0.27)	17.93 (0.13)	SWIFT (UVOT)
55742.84	29.84	15.71 (0.06)	16.79 (0.09)	18.53 (0.22)	18.12 (0.15)	SWIFT (UVOT)
55743.84	30.84	15.85 (0.06)	17.03 (0.09)	18.99 (0.29)	18.36 (0.18)	SWIFT (UVOT)
55745.25	32.25	16.01 (0.07)	17.17 (0.10)	18.81 (0.25)	18.54 (0.21)	SWIFT (UVOT)
55746.12	33.12	16.24 (0.07)	17.30 (0.11)	19.08 (0.30)	18.32 (0.17)	SWIFT (UVOT)
55750.60	37.60	16.49 (0.07)	17.51 (0.11)	18.81 (0.21)	18.78 (0.21)	SWIFT (UVOT)
55754.62	41.62	16.72 (0.07)	17.57 (0.10)	19.09 (0.26)	19.11 (0.26)	SWIFT (UVOT)
55758.55	45.55	16.69 (0.08)	17.75 (0.12)		19.00 (0.25)	SWIFT (UVOT)
55762.57	49.57	16.90 (0.10)	17.58 (0.12)	18.85 (0.24)	18.74 (0.22)	SWIFT (UVOT)
55766.52	53.52	16.68 (0.08)	17.79 (0.13)	19.10 (0.26)	18.80 (0.21)	SWIFT (UVOT)
55770.80	57.80	16.62 (0.07)	17.70 (0.12)	18.97 (0.23)	18.96 (0.24)	SWIFT (UVOT)
55775.69	62.69	16.55 (0.07)	17.72 (0.12)	19.14 (0.30)	18.89 (0.24)	SWIFT (UVOT)
55780.50	67.50	16.70 (0.08)	17.88 (0.14)	19.30 (0.36)	19.37 (0.37)	SWIFT (UVOT)
55784.80	71.80	16.52 (0.07)	17.95 (0.15)	19.11 (0.32)	18.61 (0.23)	SWIFT (UVOT)
55788.74	75.74	16.44 (0.07)	17.85 (0.12)	19.36 (0.37)	18.92 (0.22)	SWIFT (UVOT)

Table 13. List of optical and NIR spectroscopic observations.

JD (+2400000)	Phase (d)	Grism	Range (Å)	Resolution	Resolution (Å)	Instrument
55716.41	3.41	?	?	?	?	TNG (LRS)
55716.47	3.48	IJ	9000-14500	333		TNG (NICS)
55716.49	3.50	HK	14000-25000	333		TNG (NICS)
55718.42	5.42	Grism 4	3200-9100	355	16.2	NOT (ALFOSC)
55718.44	5.44	Grism 5	5000-10250	415	16.8	NOT (ALFOSC)
55719.40	6.40	Grism 4	3200-9100	355	16.2	NOT (ALFOSC)
55719.42	6.42	Grism 5	5000-10250	415	16.8	NOT (ALFOSC)
55721.39	8.39	Grism 4	3200-9100	355	16.2	NOT (ALFOSC)
55721.40	8.40	Grism 5	5000-10250	415	16.8	NOT (ALFOSC)
55722.57	9.57	R300B	3200-5300		4.1	WHT (ISIS)
55722.57	9.57	R158R	5300-10000		7.7	WHT (ISIS)
55722.42	9.42	IJ	9000-14500	333		TNG (NICS)
55722.46	9.48	HK	14000-25000	333		TNG (NICS)
55725.38	12.38	R300B	3200-5300		4.1	WHT (ISIS)
55725.38	12.38	R158R	5300-10000		7.7	WHT (ISIS)
55730.45	17.45	Grism 4	3200-9100	355	16.2	NOT (ALFOSC)
55730.46	17.46	Grism 5	5000-10250	415	16.8	NOT (ALFOSC)
55730.52	17.52	IJ	9000-14500	333		TNG (NICS)
55730.57	17.57	HK	14000-25000	333		TNG (NICS)
55733.42	20.42	Grism 4	3200-9100	355	16.2	NOT (ALFOSC)
55733.43	20.43	Grism 5	5000-10250	415	16.8	NOT (ALFOSC)
55737.68	20.43	200 H+K	14900-24000	1881(H)/2573(K)		LBT (LUCIFER) !Check!
55738.49	25.49	Grism 4	3200-9100	355	16.2	NOT (ALFOSC)
55738.50	25.50	Grism 5	5000-10250	415	16.8	NOT (ALFOSC)
55738.41	24.41	IJ	9000-14500	333		TNG (NICS)
55743.40	30.40	Grism 4	3200-9100	355	16.2	NOT (ALFOSC)
55743.44	30.44	Grism 5	5000-10250	415	16.8	NOT (ALFOSC)
55748.40	35.40	Grism 4	3200-9100	355	16.2	NOT (ALFOSC)
55748.41	35.41	Grism 5	5000-10250	415	16.8	NOT (ALFOSC)
55748.39	35.39	IJ	9000-14500	333		TNG (NICS)
55748.42	35.42	HK	14000-25000	333		TNG (NICS)
55753.41	40.41	Grism 4	3200-9100	355	16.2	NOT (ALFOSC)
55753.43	40.43	Grism 5	5000-10250	415	16.8	NOT (ALFOSC)
55757.39	44.39	Grism 4	3200-9100	355	16.2	NOT (ALFOSC)
55757.41	44.41	Grism 5	5000-10250	415	16.8	NOT (ALFOSC)
55758.39	45.39	IJ	9000-14500	333		TNG (NICS)
55758.42	45.42	HK	14000-25000	333		TNG (NICS)
55762.39	49.39	Grism 4	3200-9100	355	16.2	NOT (ALFOSC)
55762.40	49.40	Grism 5	5000-10250	415	16.8	NOT (ALFOSC)
55765.40	52.40	Grism 4	3200-9100	355	16.2	NOT (ALFOSC)
55765.42	52.42	Grism 5	5000-10250	415	16.8	NOT (ALFOSC)
55765.39	52.39	IJ	9000-14500	333		TNG (NICS)
55765.42	52.42	HK	14000-25000	333		TNG (NICS)
55771.41	58.41	?	?	?	?	CA (CAFOS)
55780.39	67.39	Grism 4	3200-9100	355	16.2	NOT (ALFOSC)
55780.43	67.43	zJ	?	700		WHT (LIRIS)
55780.40	67.40	HK	?	700		WHT (LIRIS)
55784.40	71.40	?	?	?	?	CA (CAFOS)
55795.39	82.39	?	?	?	?	CA (CAFOS)
55801.37	88.37	IJ	9000-14500	333		TNG (NICS)
55801.40	88.40	HK	14000-25000	333		TNG (NICS)
55804.36	91.36	R300B	3200-5300		4.1	WHT (ISIS)
55804.36	91.36	R158R	5300-10000		7.7	WHT (ISIS)
55812.36	99.36	?	?	?	?	CA (CAFOS)